Effect of Bond Property Between CFRP Bar and Concrete on Nonlinear Behavior of Circular CFRP Reinforced Concrete Beams

Rabotovao, A. Mamy

Miki, Tomohiro

(Citation)
Journal of Advanced Concrete Technology,21(5):380-391

(Issue Date)
2023-05-20

(Resource Type)
journal article

(Version)
Version of Record

Journal of Advanced Concrete Technology Vol. 21, 380-391, May 2023 / Copyright © 2023 Japan Concrete Institute

Scientific paper

Effect of Bond Property Between CFRP Bar and Concrete on Nonlinear Behavior of Circular CFRP Reinforced Concrete Beams

Mamy A. Rabotovao[1] and Tomohiro Miki[2*]

Received 23 December 2022, accepted 29 April 2023

doi:10.3151/jact.21.380

Abstract

Carbon fiber reinforced polymer (CFRP) bars present advantages over conventional steel rebars such as non-corrosiveness and relatively high tensile strength. CFRP bars cannot directly substitute steel rebars as the main reinforcement for concrete structures due to a lack of understanding of the behavior of CFRP-reinforced concrete (RC) members. This research investigates the effect of surface characteristics of deformed FRP bars on the bond between FRP bars and concrete. Moreover, the research aims to understand how the bond property of FRP bars affects the behavior of CFRP RC beams under shear load. An analysis was conducted for a better understanding of this matter by producing different bond models with a reproductive pull-out test that takes into consideration the surface characteristics aspect of the FRP bar. The structural analysis for CFRP RC beams using the proposed bond models was conducted. It was observed that surface characteristics of CFRP rebars affect the bond-slip curves in a way that the ribbed type presents higher bond strength and greater shear stiffness modulus than the dented type. In addition, the analysis for CFRP RC beams using a ribbed bond model tends to generate steeper diagonal cracks leading to the shear failure in the CFRP RC beams.

1. Introduction

Steel reinforcing bars are the main material for the internal reinforcement of concrete structures. However, in the presence of corrosive environments, steel reinforcing bars even in concrete may suffer severe deterioration due to corrosion limiting the life expectancy of these concrete members and leading to costly repairs and rehabilitation. Thus, much research has been carried out on controlling the corrosion of steel rebars or finding alternative materials that provide the desirable characteristics of steel rebars as well as prevent corrosion.

The use of non-corrosive materials such as fiber reinforced polymer (FRP) could be one of the solutions to that matter. FRP reinforcing bars present several advantages over conventional steel bars, mainly non-corrosiveness, high tensile strength, lightweight, fatigue resistance, nonmagnetic electrical insulation, small creep deformation, and specific gravity (Hao *et al.* 2009). Therefore, FRP bars have been used as reinforcement for different concrete structures subjected to an aggressive environment such as marine structures and bridges (Mohamed and Benmokrane 2015).

Despite the advantages of FRP bars over conventional steel reinforcement, a direct substitution between FRP and steel rebar is not possible due to differences in the mechanical and physical properties between the two materials. The main problems that prevent the use of FRP rebars on a wide scale as a reinforcing material for concrete structures are: (i) when subjected to tensile force FRP exhibits linear elastic behavior up to failure and does not show any yielding point. In other words, the FRP bar is a brittle material. (ii) The modulus of elasticity for some types of FRP is much lower than steel, hence deflection and crack widths may control the design of reinforced concrete structures.

Whether at the ultimate state (capacity) or at the serviceability limit state (crack width and deflection) the behavior of a reinforced concrete member depends on the force transfer between the reinforcement and the concrete. This force transfer depends on the bond between the two materials. Therefore, the bond property between FRP bars and concrete is a critical aspect of the structural performance of the FRP reinforced members.

Still in the topic of concrete structures in aggressive environments, concrete members with a circular cross-section are often used in bridges or marine structures as pile or fender since it provides equal strength characteristics in all directions. In the last decade, the experimental works have mainly focused on FRP reinforced concrete members with a rectangular cross-section. Hence, research related to circular carbon fiber reinforced polymer (CFRP) reinforced concrete beams or columns is a necessity (Mohamed and Benmokrane 2015).

This study aims at a better understanding of the bond between FRP bars and concrete and its effects on the structural behavior of FRP RC concrete beams. Furthermore, this study uses two different surface characteristics of FRP bars for sensitive analysis of the internal strain distribution of concrete. It was found that sand-coating surface characteristics were the ones leading to the highest load carrying capacity, and analytical specimens sustain larger deflection than

[1]Graduate Student, Department of Civil Engineering, Kobe University, Kobe, Japan.
[2]Associate Professor, Department of Civil Engineering, Kobe University, Kobe, Japan. *Corresponding author, *E-mail* : mikitomo@port.kobe-u.ac.jp

experimental ones (Rabotovao and Miki 2022). Compared to the previous article (Rabotovao and Miki 2022), this study presents a better understanding of the effect of different bond-slip parameters, such as the shape of the bar, the elastic modulus, the diameter, and the local bond property. The present study also focuses on the effect of the kinematic shape of FRP rebars as other parameters were taken as constant depending on the shape of FRP rebars.

This paper also provides details on the behavior between FRP bars and concrete on a microscopic scale allowing detailed information regarding strain and stress distribution on a small interface element between concrete and FRP bars. Moreover, the first analytical program suggests the concept of a local bond between concrete and FRP bars during pull-out test which shows strain and stress distribution. Also, this paper presents how the study on a microscopic scale can be applied to a real structural component such as circular CFRP beams. Furthermore, for the FEM part, this paper investigated two different interface elements, namely a surface interface element and a line interface element.

2. Literature review on the bond property between FRP and concrete

FRP reinforced concrete members rely on the durability of their composing materials (concrete and FRP bars) and on the bond property between concrete and FRP bars. Since used for a long period of time in the field of civil engineering, the durability of concrete is not questioned (*fib* 2010). On the other hand, FRP bars present advantageous properties that are considered durable, however, the bond between FRP bars and concrete is far from being understood.

One way to understand the bond between FRP bars and concrete is the pull-out test. This setup test consists of a block of concrete with an embedded FRP bar inside, and it allows a better understanding of the short and long-term behavior of the bond between concrete and FRP bars. The setup consists of pulling the FRP bar from the block of concrete while this latter is restrained. Precisely, the bar itself is not bonded to the concrete throughout its all length but only for a certain length called "embedded length." This test setup results in understanding the applied force (F) and the relative displacement between the concrete and the slips at the loaded section and at the free end. The applied force leads to the calculation of the bond stress between concrete and FRP bars with the following equation:

$$\tau = \frac{F}{\pi l_{emb} ø} \qquad (1)$$

where

τ : Bond stress (N/mm^2)
F : Pull-out tensile force (N)
l_{emb} : Embedded length in concrete (mm)
ø : Diameter of the bar (mm)

The bond strength is defined as the maximum bond stress observed on the bond-slip curve obtained by the precedent equation. The bond strength between concrete and FRP bars depends on the embedment length, the diameter of the bar, the nature of the bar, and its surface treatment.

The following presents the effect of different parameters on the bond strength and bond behavior between FRP bars and concrete after consideration of 1002 pull-out tests (Nepomuceno *et al.* 2021). Unlike steel reinforcing bars, FRP bars are composed of a wrapping matrix and fibers leading to a lower modulus of elasticity and lower stiffness. Previous research (Aiello *et al.* 2007; Baena *et al.* 2009; Nepomuceno *et al.* 2021) has reported that a type of fiber influences the bond strength between FRP bars and concrete. The collected data has reported the effect of three types of FRP bars, namely BFRP (B: Basalt), CFRP (C: Carbon), and GFRP (G: Glass).

The experiment showed that BFRP bars presented a higher bond strength than CFRP bars and GFRP bars. Regarding the modulus of elasticity, CFRP bars presented a higher modulus of elasticity than those of BFRP and GFRP bars, whereas CFRP bars presented a lower performance than BFRP and GFRP bars since no bar rupture is observed during pull-out tests (Nepomuceno *et al.* 2021). This failure mode of CFRP bars in the direct pull-out test could be advantageous for the FRP RC beam since reinforcement would not contribute to additional cracks in the concrete. The collected data takes into consideration 15 different embedment lengths ranging from 2ø to 20ø, where ø is the nominal diameter of the FRP bars. Among those embedment lengths, the use of 5ø is the most common one, representing up to 48% of specimens. Moreover, this embedment length of 5ø is the suggested value in international guidelines for bond characterization of FRP bars to concrete (ACI 2015; ASTM 2020; CNR 2007; CSA 2012).

In addition, it was reported that the bond strength decreases with the embedment length (Achillides and Pilakoutas 2004; *fib* 2007, El Refai *et al.* 2015) due to a decrease in the friction effects along the length. This reduction of friction is the consequence of Poisson's ratio effects represented by a reduction in the radial direction while the bar elongated along its length (*fib* 2007).

The bond stress between concrete and FRP bars can be explained with three different mechanisms: chemical adhesion, mechanical interlocking, and frictional bond. Chemical adhesion is defined as the resistance that leads to the separation of materials of different natures (concrete, FRP matrix). On the other hand, mechanical interlocking is related to the shape and deformation of the FRP bar that generates localized forces when slipping occurs. And the last mechanism is created by the existence of the surface contact of concrete and FRP bars. Hence, the surface treatment plays a significant role in good bond performance. Therefore, Nepomuceno *et al.* (2021) presented different techniques, including sand coating, surface deformations (helical wrapping, indentation), or a combination of both techniques recently, and reported the influence of different surface treatments of FRP bars. The FRP bars were subdivided into four groups, namely: sand-coating with a deformed surface (SC+DS), deformed surface (DS), sand coating (SC), and smooth surface (SM). These different surface treatments were considered with an embedment length of 5ø. From the experiments, it was found that FRP bars with surface treatment present a higher bond strength than smooth bars, thus a better bond performance.

3. Analytical programs

3.1 Analysis for pull-out tests of FRP bar embedded in concrete

The analytical model of the pull-out test is targeted for experimental results performed by Solyom and Balázs (2020). The specimens were designed by taking into consideration ACI, CSA, and RILEM recommendations. Each specimen consists of a cubic mold of 150 mm with an FRP bar embedded in the center. The embedment length was taken as 5ø. This analytical program takes into consideration the shapes of deformed surfaces. FRP bars with ribs and indentation are shown in **Fig. 1**.

As shown in **Fig. 1**, the face of the specimen is fixed along the direction of the loading (X-axis). The bottom edge of the specimen is fixed along the Y- and Z-axes to prevent any displacement or rotation. In addition, two types of bars are used in the analysis; a bar with rib and a bar with indentation referred to as a ribbed bar and a dented bar, respectively. The dimensions of rib and indentation are taken from experimental specimens, namely R10-In-12-G-P5 and R12-Rb-12-G-P6 (Solyom and Balázs 2020). The height and width of the rib of the ribbed bar were 0.74 mm and 3.54 mm, respectively, and will be referred to as a large rib or a large indentation in the following analysis. The depth and width of the indentation of the dented bar were 0.46 mm and 1.84 mm, respectively, and will be referred to as a small rib or a small indentation.

DIANA ver. 10.5 was used to model the specimens for the pull-out tests. Regarding the meshing of the embedded part of the CFRP bar, the ribbed part and dented part were modeled with a fine mesh size of 0.5 mm. The other surface of the bar presents a mesh size of 1.5 mm. Such discretization was considered to represent the interlock mechanics between ribs or indentation and concrete cover. The different angles of indentation or rib are considered in the parametric study. The angle corresponds to a spacing of indentation or rib, r_s as shown in **Fig. 1**.

For the tensile behavior of concrete, a bilinear tensile model characterized by a plateau after the tensile strength is reached, was considered with a tensile strength of 2.5 N/mm^2. For the compressive behavior, a bilinear model with a plateau was considered as well with a compressive strength of concrete as 36 N/mm^2 corresponding to an elastic modulus of 30000 N/mm^2. CFRP bar was modeled with an elastic model. The only parameter taken into consideration was the elastic modulus of CFRP rebars 141000 N/mm^2.

The interface between concrete and FRP bars was modeled as a 3D surface element. The shear stiffness modulus and the normal stiffness modulus of the interface are calculated by the following equations, which are based on the parametric analysis.

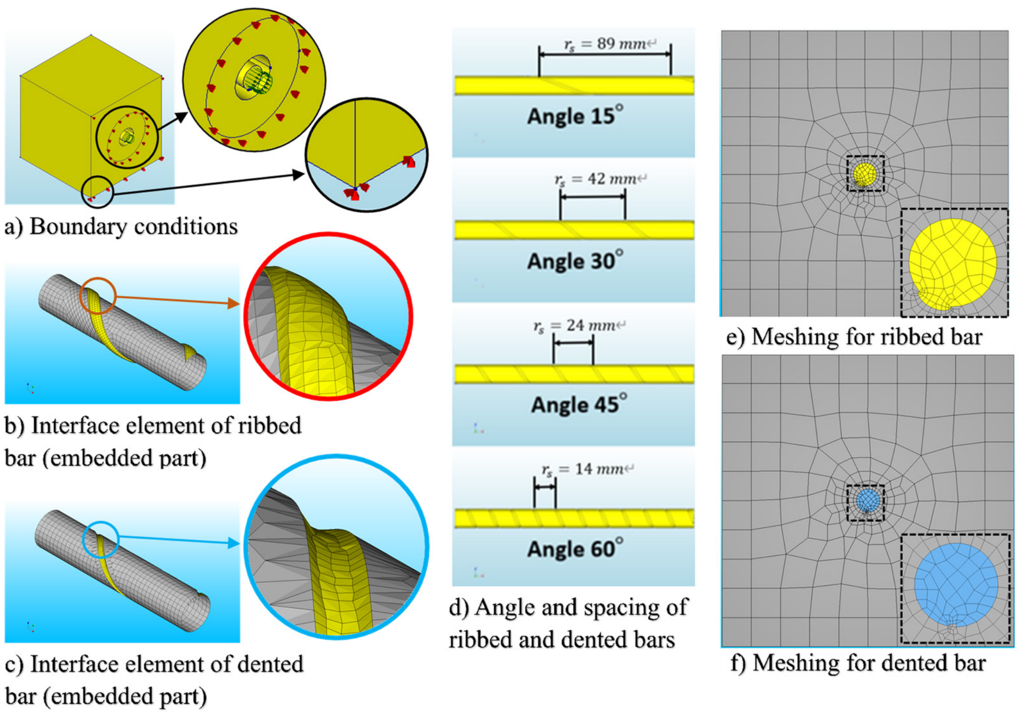

Fig. 1 Representative model for pull-out test.

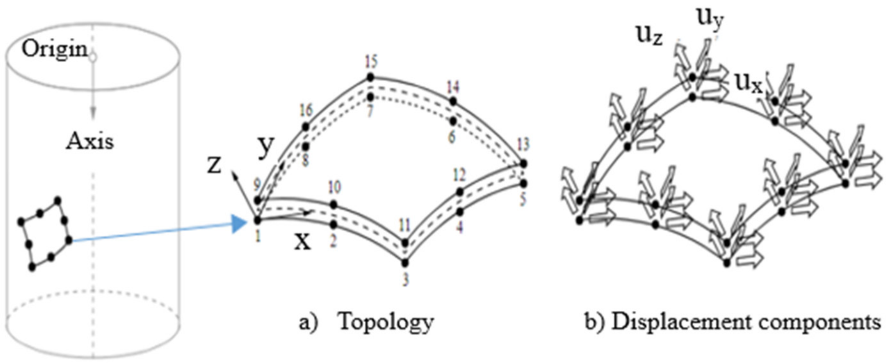

Fig. 2 One interface element of the surface of the FRP bar.

$$K_{tt} = \frac{K_{nn}}{1000} \tag{2}$$

$$K_{nn} = E / (t \times N) \tag{3}$$

where

K_{tt} : shear stiffness modulus (N/mm³)
K_{nn} : normal stiffness modulus (N/mm³)
E : elastic modulus of concrete (N/mm²)
t : thickness of the interface element
N : number of interface elements

For simplicity in the calculation of those stiffnesses mentioned above, the thickness of the interface element is assumed to be 1 mm.

The interface between concrete and FRP bars consists of a surface interface composed of interface elements, as shown in **Fig. 2**. The nonlinearity of the interface elements is controlled by a diagram that introduces the concept of a local bond. The local bond is associated with each interface element of the surface interface. A maximum local shear stress is defined for which the connection breaks. Once this local shear stress in the element interface has reached the limit in the respective direction, the stiffness in all directions in the element interface will reduce. **Figure 2** shows the relationship between the global coordinate system XYZ and the local coordinate system xyz of the surface interface, where, for each node of an interface element, the x- and y-axes are directed in the plane of the surface interface and the z-axis is perpendicular to that surface. However, displacements and shear tractions are calculated in the global system XYZ. The local bond was introduced as a bilinear curve in this study.

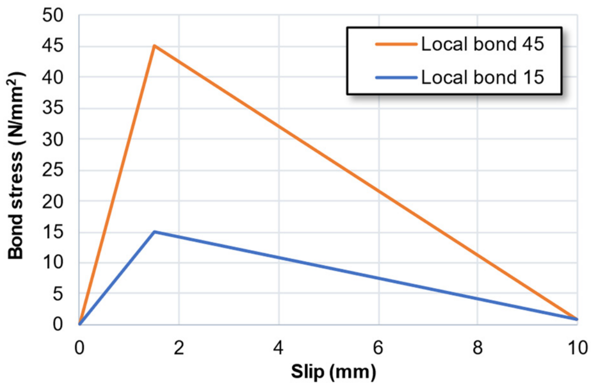

Fig. 3 Local bond parameter on each interface element.

As shown in **Fig. 3**, two different local bond diagrams were considered here; the first one, "local bond 15" is fitted to the averaged bond stress-slip relationship of the experiment by Solyom and Balázs (2020), and the second one, "local bond 45" was selected to observe the effect of an increase in local bond on the overall bond-slip curves. The exaggerated value of a local bond of 45 N/mm² is considered a trial since in experimental studies, the bond is defined as a mean value of traction force other than the surface in contact between FRP bars and concrete. This implies that the shear traction on every part of the interface between the concrete and FRP bar is not uniform or equal to that mean value.

3.2 Analysis for CFRP RC beams with a circular cross-section

This study aims at understanding the behavior of circular cross-sectional CFRP RC beams under shear. As an analytical design, specimens consist of circular beams with a diameter of 500 mm and a total length of 3000 mm (Mohamed *et al.* 2017). Specimens were reinforced with sand coated CFRP longitudinal rebars (16 mm dia.) and CFRP spiral (12 mm dia.) with different spacings of 100 mm, 150 mm, and 200 mm.

Regarding the boundary conditions, each specimen is simply supported other a length span of 2400 mm. The load is applied as displacement control in the Z direction. The left support is fixed in all directions; however, the right support is fixed in Y- and Z-axes.

DIANA ver. 10.5 was used to model those specimens. In the analysis, several bond models of CFRP rebars are associated with the longitudinal reinforcing bars. The concrete was modeled with solid elements with a mesh size of 50 mm. The total strain crack model is considered. The behavior of concrete in compression was modeled using a parabolic model (Feenstra 1993). The compressive fracture energy of concrete G_C is one of the main parameters and was determined using Eq. (4) (Yamaya *et al.* 1999). The compressive strain of concrete was 36 N/mm^2. The reduction of the compressive strength of concrete due to lateral cracking is also taken into consideration (Vecchio and Collins 1993). After cracking, an exponential tension softening model is considered (Hordijk 1991). The tensile fracture energy G_F is calculated with Eq. (5) and was obtained according to the JSCE standard specification for concrete structures (JSCE 2002). The tensile strength of concrete was set to 2.5 N/mm^2.

$$G_C = 8.77\sqrt{f_c'} \tag{4}$$

$$G_F = 10\left(d_{max}\right)^{1/3} . f_c'^{1/3} \text{ with } d_{max} = 20\,mm \tag{5}$$

where
G_C : compressive fracture energy of concrete (N/mm)
G_F : tensile fracture energy of concrete (N/mm)
f_c' : compressive strength of concrete (N/mm^2)
d_{max} : maximum size of aggregate (mm)

Figure 4 presents the details of the analytical specimens, including the boundary conditions, the mesh discretization, and the disposition of reinforcements. Regarding the boundary conditions, each specimen is supported by two supports, where the left support is restrained in all directions, although the right one is restrained in the direction of Y- and X-axes. The diameter of the longitudinal CFRP rebar (number of longitudinal rebars: 16) was 16 mm with an elastic modulus of 141000 N/mm^2 and a tensile strength of 1659 N/mm^2. The spiral consisted of CFRP bar with a diameter of 12 mm and an elastic modulus of 124000 N/mm^2, and a tensile strength of 1562 N/mm^2.

4. Results of the representative model for pull-out test

To understand the bond behavior of those new materials, different parameters are considered: an angle of indentation, an angle of rib, a size of indentation and rib, a diameter of rebar, and the modulus of elasticity of FRP rebars which represented for GFRP and CFRP rebars. In the parametric analysis, the local bond model with 15 N/mm^2 was used in sections from 4.1 to 4.4.

4.1 Effect of indentation of FRP bar on bond-slip curves

This section shows the effect of an indentation of FRP bar on the bond-slip curves, especially an effect of the angle and the size of indentation, as shown in **Fig. 5**. Analytical

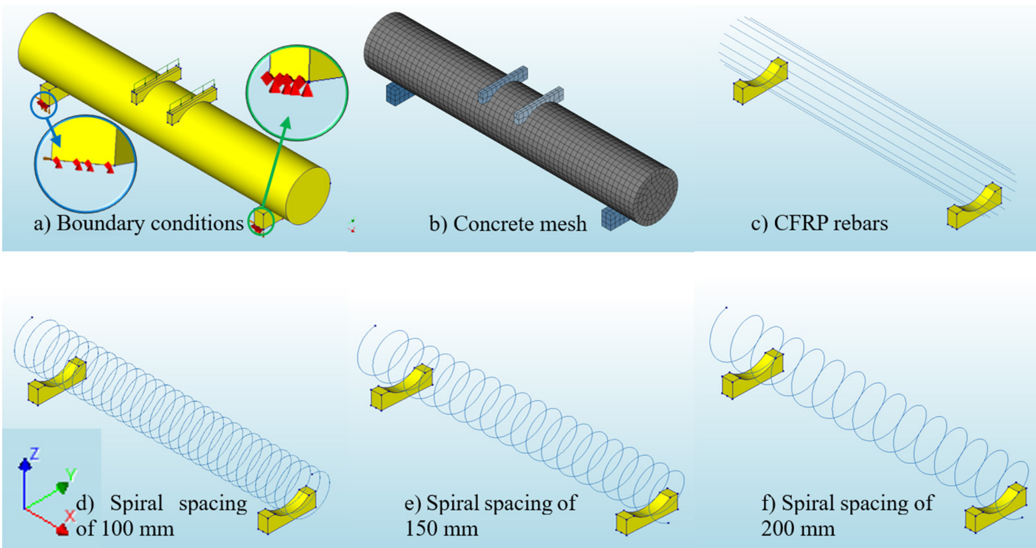

Fig. 4 Modeling for CFRP RC beams with different spiral spacings.

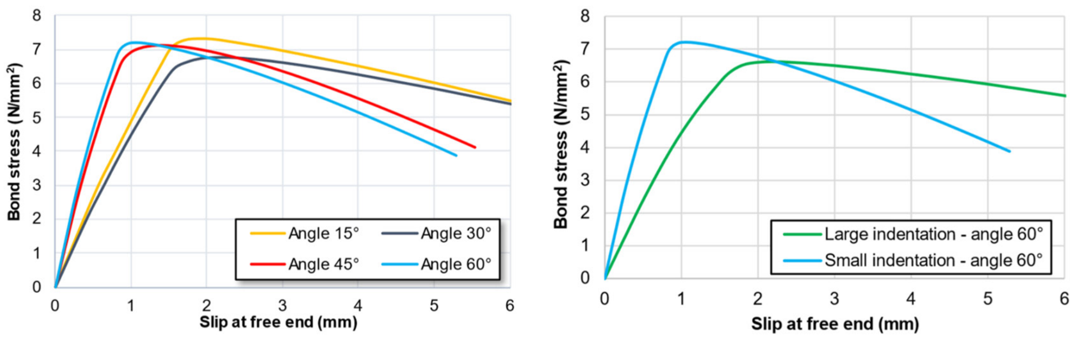

(a) Effect of different angle of indentation (b) Effect of the size of indentation

Fig. 5 Effect of indentation on the bond-slip curves between FRP (12 mm bar) and concrete.

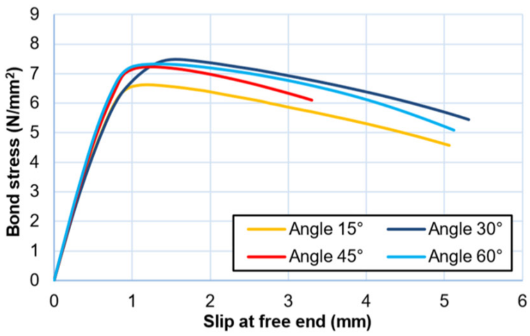

(a) Effect of different angle of rib

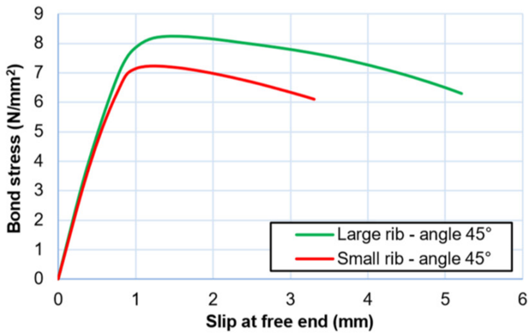

(b) Effect of different size of rib

Fig. 6 Effect of ribs on the bond-slip curves between FRP (12 mm bar) and concrete.

results show that dented bar with angles of indentation of 15° and 30° leads to a large slip at the maximum stress of 1.88 mm and 2.27 mm, respectively, as presented in **Fig. 5(a)**. This is because of the almost uniform and smooth surface all along the embedded part. On the other hand, larger angles of indentation, such as 45° and 60°, generate smaller slips at the maximum stress of 1.33 mm and 1.06 mm, respectively. The different angles of indentation in the later cases do not affect the bond strength since no actual difference was observed. However, it significantly affects the stiffness modulus, which indicates a slope of the bond-slip curve of those specimens. Therefore, in the case of the dented specimen, the angle of 60° is considered the suitable angle since it is the one that leads to the highest stiffness modulus.

To observe the effect of the size of indentation, the following two different types of dented bars are considered:

i) Bar with small indentation: a depth of 0.46 mm and a width of 1.84 mm and,
ii) Bar with larger indentation: a depth of 0.74 mm and a width of 3.54 mm.

Regarding the size of the indentation, a larger and a smaller indentation were both associated with an angle of indentation of 60° since it presents the highest stiffness modulus. The diameter of both bars was set 12 mm in this analysis.

The bond-slip curves at the free end of these bars are shown in **Fig. 5(b)**. It is obvious that smaller indentation presents the lower slip and higher bond strength, corresponding, of course, to a larger shear stiffness modulus. In the model, it is assumed in the analysis that the angle of the rib or indentation was increased with decreasing the spacing. For a dented bar, it is also assumed that the smaller width and depth of the indentation, the larger the round surface except for the indentation of the bar which is in contact with the concrete in the analytical model. The slip at the concrete interface may occur when large shear traction stresses lead to large strain reaching the zone of indentation. Since smaller indentation provides larger round surface contact between concrete and bars, the bond stress-slip relationship of the dented bar with a large indentation and 60° angle indicated similar to that of the dented bar with a small indentation and an angle of 15 to 30 degrees.

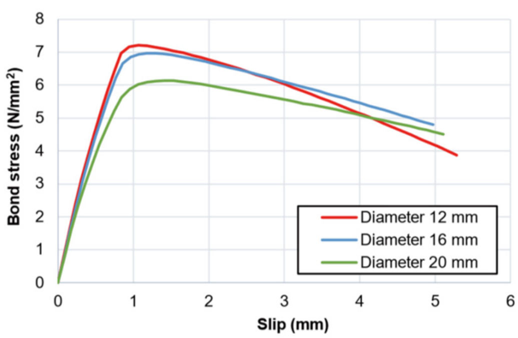

Fig. 7 Effect of different diameters on the bond between dented GFRP bar and concrete.

4.2 Effect of ribs on the bond-slip curves between FRP and concrete

Among the four different angles of ribs, the angle of 45° provides the fittest result in the case of ribbed specimens as shown in **Fig. 6(a)**. **Figure 6(b)** shows the bond between FRP bars and concrete tends to increase with the enlargement of the size of the rib. In addition, regarding the size of ribs, the following dimensions were considered:

i) Bar with small rib: 0.46 mm rib height and 1.84 mm rib width and,
ii) Bar with larger rib: 0.74 mm rib height and 3.54 mm rib width.

4.3 Effect of diameters on the bond-slip curves between FRP and concrete

Figure 7 shows that the bond between FRP bars and concrete decreases with the increase in diameter. The diameter affects the bond strength of each pull-out test. Based on **Fig. 7**, it is analytically found that the bond between FRP bars and concrete decreases with the increase in diameter. There is no significant difference regarding the slip at the maximum bond stress and the diameter affects mainly the bond strength of each pull-out test.

4.4 Effect of the modulus of elasticity of FRP bars

Figure 8 shows how different moduli of elasticity of FRP

Table 1 Comparison between experimental and analytical results.

Designation	Bond strength (N/mm^2)	Slip at max. stress (mm)	Stiffness (N/mm^3)
Small indentation – Local bond 15	7.29	1.88	3.88
Small indentation – Local bond 45	12.14	1.11	10.93
Specimen R10-In-12-G-P5 in the study of Solyom and Balázs (2020)	15.13	1.56	9.88

bars affect the bond-slip curve between FRP bars and concrete. The module of elasticity of the GFRP bar and CFRP bar used in this section are 45000 N/mm^2 and 141000 N/mm^2, respectively, and for both bars, a Poisson ratio of 0.2 was set. Those bars are dented bars with the same angle of indentation of 60°. **Figure 8** shows that among the different parameters that can affect the bond-slip curves between concrete and FRP bars, the elastic modulus is not a predominant one since almost similar bond-slip curves are observed, though an increase in the elastic modulus was clearly taken into consideration. In this study, an embedment length of 5ø (ø: nominal diameter) was considered, which may lead to those results.

The bond-slip curves of different elastic modulus values are identical since the failure of the specimen is a concrete failure but not the bar failure. It just shows that the elastic moduli of those bars are not a predominant parameter regarding their bond-slip curves.

4.5 Effect of different local bond curves on the overall bond-slip curves

In the parametric analysis shown previously, the local bond was considered in the analysis, where the bond strength ranges from around 7 to 8 N/mm^2. **Figure 9** shows that the results of bond stress of the dented bar model with a diameter 12 mm changed from 7.3 N/mm^2 up to 12.1 N/mm^2 in which the local bond stress has ranged from 15 N/mm^2 and even up to 45 N/mm^2. Here, the stress traction distribution of local shear stress shows that it is not uniformly distributed over the interface element as shown in **Fig. 10**. This non-uniform distribution of the local bond stress is the reason why an increase in the local bond stress from 15 N/mm^2 up to 45 N/mm^2 results only in the increase of 166% in the bond strength of the pull-out specimen in the analysis. The analytical results and the results in the case of the experimental specimen R10-In-12-G-P5 in the study of Solyom and Balázs (2020) are summarized in **Table 1**. These results indicate that the stiffness of the analytical results was similar to that of the experimental one. Therefore, in the following analysis, this local bond of 45 N/mm^2 is considered for the bond model for CFRP bars with a diameter of 16 mm.

4.6 Bond models of CFRP bar with a diameter of 16 mm and different surface characteristics

This section presents the bond models obtained from this representative model for the pull-out test, which will be used as parameters in new sets of analyses. Based on the

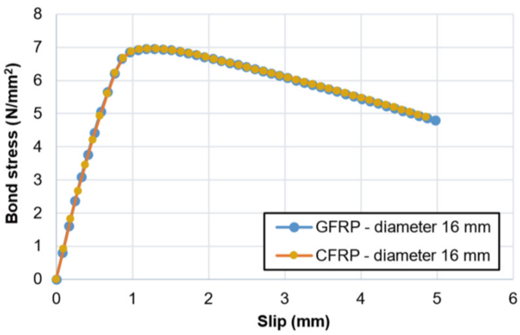

Fig. 8 Effect of elastic modulus on the bond between dented FRP bar and concrete (angle of indentation: 60°).

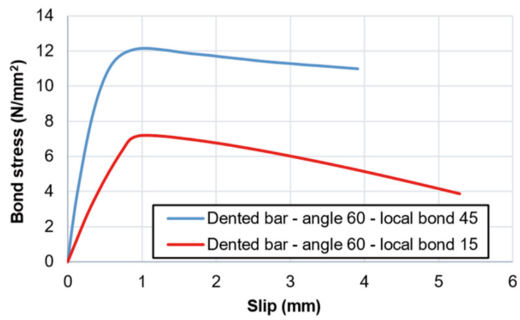

Fig. 9 Effect of local bond on the bond slip curve of dented bar (diameter 12 mm).

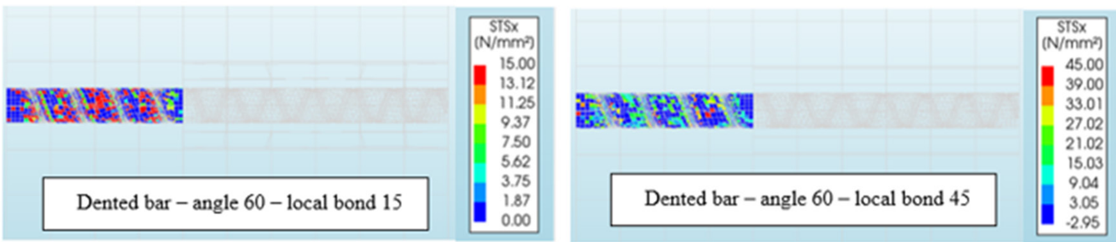

Fig. 10 Distribution of the shear traction on the surface interface element for two different local bond models at the peak load.

previous experiments, a larger rib associated with an angle of 45° is presented as the highest stiffness modulus for the ribbed bar. On the other hand, a smaller indentation with an angle of 60° shows the highest stiffness modulus for the dented bar. Therefore, those two types are considered with the modulus of elasticity of CFRP rebars and a diameter of 16 mm.

Regarding the initial stiffness of those two models, the dented bond model presents an initial slip of 0.162 mm at the bond stress of 2.13 N/mm^2. On the other hand, the ribbed bond model presents an initial slip of 0.006 mm at the bond stress of 2.16 N/mm^2. Therefore, initial stiffnesses used in the analyses for those models were set as 336 N/mm^3 for the ribbed bond model and 13 N/mm^3 for the dented bond model, respectively.

Figure 11 shows the bond-slip curves of the two different models. For both surface characteristics, the bond-slip curves are composed of an initial slope followed by a plateau. These bond-slip curves were used as the linear interface parameters between CFRP bars and concrete in the structural analysis of CFRP RC beams.

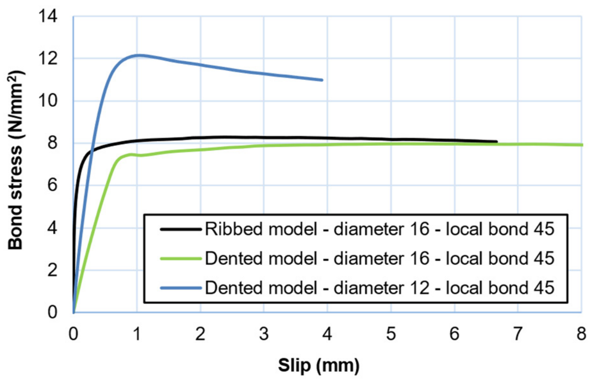

Fig. 11 Bond models used in the analysis for the CFRP RC beams.

5. Results of the CFRP RC beams

5.1 Load carrying capacity

Figure 12 shows the load-deflection curves of different BC specimens, including the experimental results (Mohamed *et al.* 2017). It is obvious that there is a difference in terms of stiffness between the experimental results and analytical results. However, the elastic behavior of the specimens was observed in both cases (experimental and analytical). The experimental specimen BC100 reached a load carrying capacity of 1270 kN corresponding to a deflection of 26 mm.

In general, the behavior of CFRP RC beams can be divided into two stages. Prior to the flexural cracking, all the beams present the same behavior, corresponding to the load of 125 kN. This stage represents the behavior of uncracked beams with the gross moment of inertia of the concrete cross-section. After cracking, an almost linear behavior is observed in almost all cases, regardless of the nature of the surface characteristics of the CFRP rebars. At this stage, a reduction of stiffness up to failure can be observed. Assuming that in the post cracking stage, the beam stiffness mainly depended on the axial stiffness of the reinforcing bars. The strength of the beam depended on its reinforcements after the cracking.

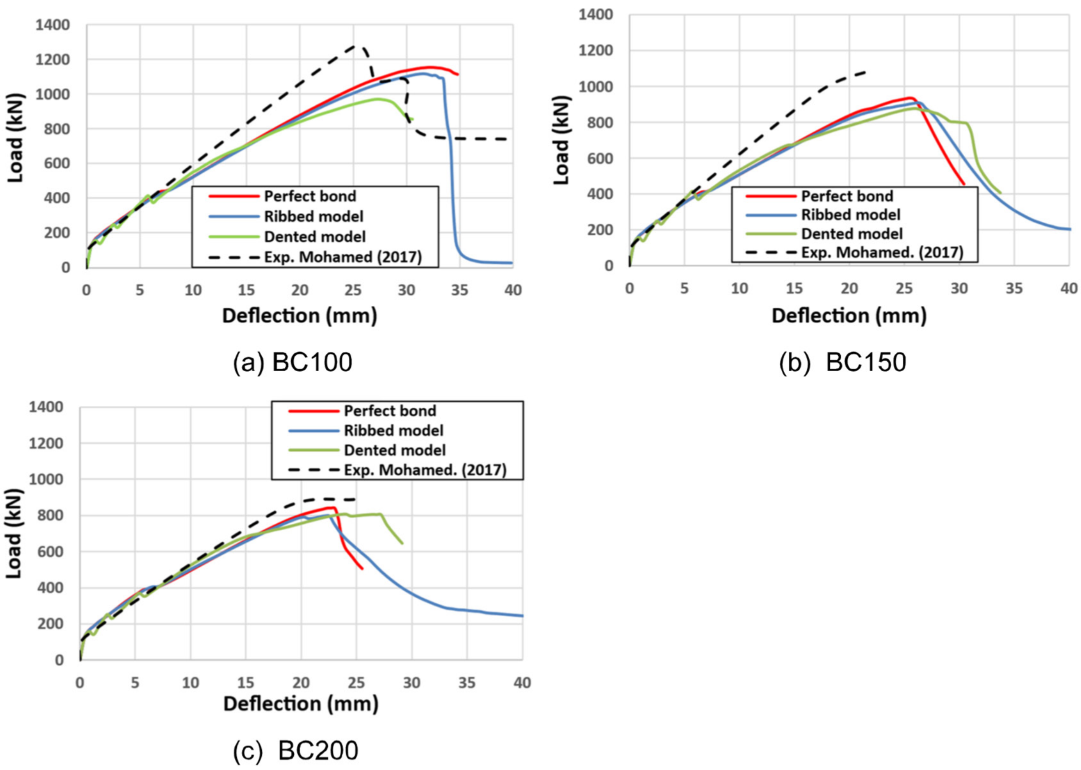

Fig. 12 Deflection curves of all BC specimens (BC100, BC150 and BC200).

Table 2 Tensile strains of longitudinal reinforcements at the midspan (tensile reinforcement).

Specimens	Perfect bond	Ribbed	Dented	Experimental results of Mohamed *et al.* (2017)
BC100	0.0090	0.0086	0.0076	0.0089
BC150	0.0071	0.0071	0.0070	0.0085
BC200	0.0063	0.0061	0.0060	0.0069

In the case of BC100, the load carrying capacities in the analysis were respectively 1155 kN, 1117 kN, and 970 kN for rebars with the perfect bond, the ribbed rebar, and the dented rebar models. Those load-deflection curves of BC 100 and BC specimens show that the nature of the bond between CFRP bars and concrete affects relatively the flexural stiffnesses of the specimen and therefore the nature of the reinforcement should be taken into great consideration in the design of FRP RC structures.

This pattern is also observed in the cases of BC150 and BC200 since the perfect bond model cases present the highest peak load followed by the ribbed model case, and the lowest load carrying capacity is observed for the case of the dented model.

5.2 Tensile strain of longitudinal CFRP rebars (BC100, BC150, and BC200)

This section presents the tensile strain of longitudinal CFRP bars obtained in the analysis at the peak load in the midspan of the tensile reinforcement. As shown in **Table 2**, the analytical tensile strains of longitudinal rebars are 0.0090, 0.0086, and 0.0076 for the perfect bond model, ribbed model, and dented model, respectively. As for the other specimens BC150 and BC200, the difference in the tensile strain distribution shows the unequal contribution of the longitudinal reinforcements after the cracking of concrete. Those values suggested that the perfect bond model presented a large force transfer among the different surface characteristics. On the other hand, dented longitudinal rebars show less contribution to the shear strength of those specimens.

Regarding the different surface characteristics, the dented bond model which presents the lowest shear stiffness modulus leads to larger slip between concrete and CFRP longitudinal rebars which reduces the force transfer between those materials, leading to a low load carrying capacity of BC100 reinforced with dented CFRP rebar.

The internal strain at the midspan of the longitudinal CFRP bar with a perfect bond model is similar to the strain of CFRP bars in the experiment. However, the load-deflection curve of the analytical specimen shows a low stiffness if compared to the experimental results.

5.3 Cracking patterns of BC specimens (BC100, BC150, and BC200)

This section focuses on analyzing the effect of different surface characteristics of longitudinal CFRP rebar on the crack propagation of circular RC beams with spiral CFRP. To observe that crack propagation, the cracking of circular beams at two different loading stages is shown in this section. Those two different loading stages are namely: the loading of 400 kN corresponding to the opening of the diagonal crack and the peak load of each specimen.

Figure 13 shows the cracking patterns of BC100 at a loading of 400 kN for different surface characteristics. BC100 with the ribbed model showed several flexural cracks with the opening of diagonal cracks in the shear span of the beam. On the other hand, BC100 with the dented model showed few large flexural cracks due to the poor bond between CFRP and concrete. Regarding specimen BC100 with the perfect bond model, several flexural cracks are also observed, as well as the opening of diagonal cracks. However, if the results of the ribbed model and the perfect-bond model are compared, the former represents more flexural cracks.

Figure 14 shows the cracking patterns of specimen

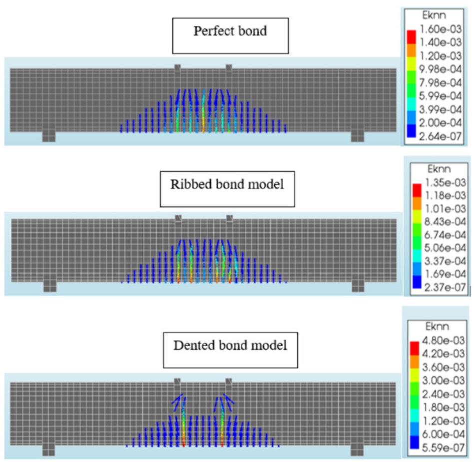

Fig. 13 Cracking patterns of BC100 at P = 400 kN.

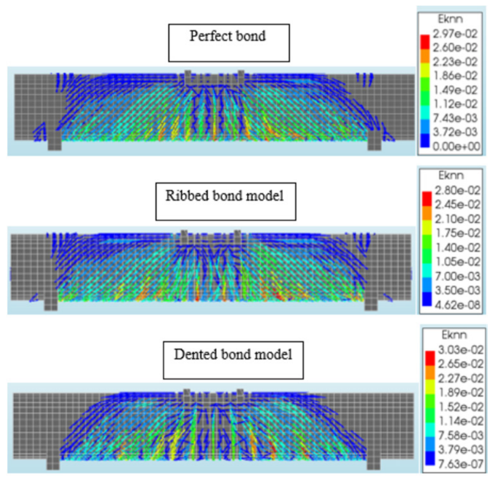

Fig. 14 Cracking patterns of BC100 at the peak load.

BC100 for experimental and analytical programs. The cracking patterns of analytical BC100 specimens at the peak load are similar to the cracking pattern of experimental BC100. Compared to the previous stage, there is no appearance of new diagonal cracks for all the specimens. Moreover, flexural cracks keep opening for all the specimens. Specimens BC 100 with perfect bond and ribbed bond model failed after the appearance of several diagonal cracks. However, specimen BC100 with the dented model shows a brittle shear failure or even a bending failure since the non-existence of real diagonal cracks joining the support and the loading point. There is no real difference between the cracking pattern of the perfect bond case and the ribbed model case since the latter provides enough bond and force transfer between CFRP bars and concrete to allow a similar cracking pattern.

Figures 15 and **16** show the cracking patterns of BC150 and BC200 at peak load. The same conclusion observed from **Fig. 14** can be drawn again from these figures.

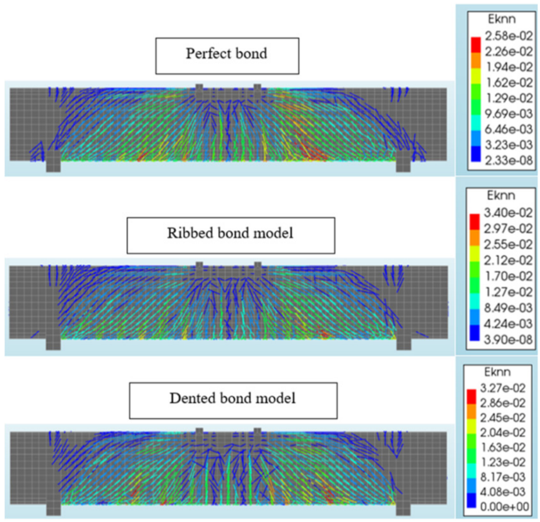

Fig. 15 Cracking patterns of BC150 at the peak load.

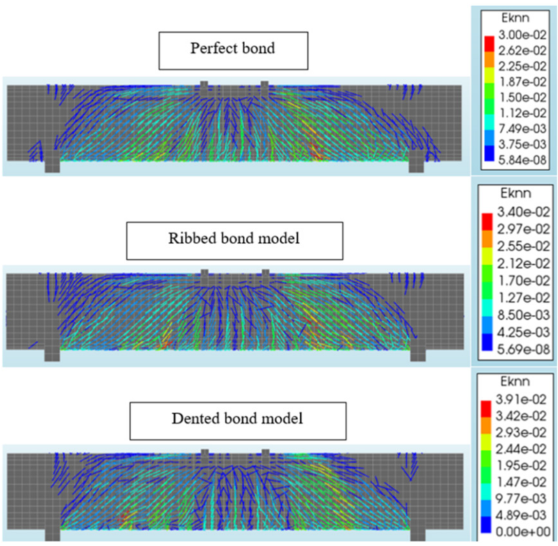

Fig. 16 Cracking patterns of BC200 at the peak load.

5.4 Discussion on the internal strain of concrete

This section describes the effect of different surface characteristics of longitudinal rebars on the internal strain of concrete in the principal direction. To do so, the internal strain of concrete at a certain loading is shown below, in this case, loading of 800 kN. Moreover, the internal strain of concrete strain are localized at three different plane sections as shown in **Fig. 17**:

i) Plane 1: The middle axial section of concrete
ii) Plane 2: The vertical section located at the distance of D/4, and
iii) Plane 3: The vertical section located at the distance of D/8, where D is the diameter of the circular beam.

In terms of the shape of the internal strain, the perfect bond model and ribbed bond model led to a similar consequence. The internal strain of concrete is mainly concentrated in the shear span of the beam.

Figures 18, **19**, and **20** present the maximum principal strain of concrete for BC100. Regarding the internal strain of concrete in the web of the CFRP RC beam, it was observed that specimens strengthened by CFRP longitudinal rebar with the perfect bond model showed

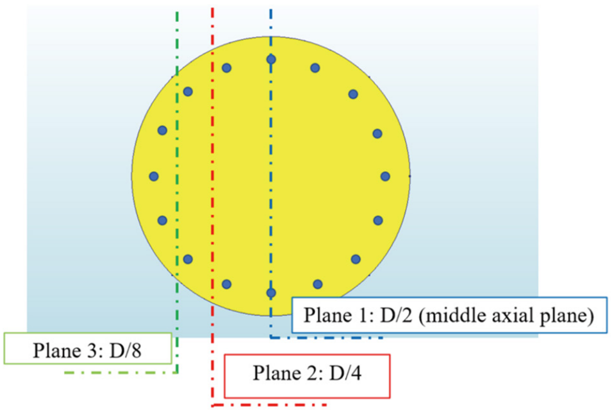

Fig. 17 Section planes of internal strain of concrete.

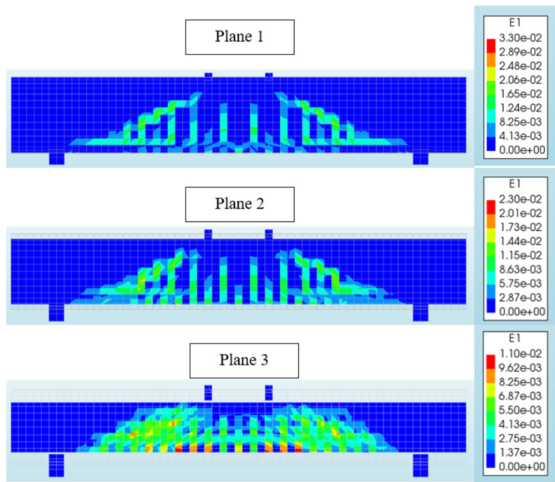

Fig. 18 Internal strain of concrete (BC100 with perfect bond).

diagonal shear cracks is clearly observed, as shown in **Fig. 18**. On the other hand, the internal tensile strain of concrete of the beams with the ribbed model, the diagonal shear cracks are observed as shown in **Fig. 19**. The perfect bond model and the ribbed model present almost the same pattern regarding the internal strain which indicates a diagonal shear strain distribution joining the support and the loading point as shown in **Figs. 18** and **19**, respectively. However, in the case of dented models, the diagonal shear strain presented a steeper angle. Moreover, those diagonal strains started from the midspan of the beam to the loading point, as shown in **Fig. 20**.

Another aspect of the surface characteristic of the bond model is mentioned hereafter. In the case of the perfect bond model, its mainly represented by an almost zero-slip displacement between longitudinal CFRP rebars and concrete. The perfect bond model can be associated with a bond model with an infinite shear stiffness modulus. Therefore, the internal strain of those two surface characteristics is the consequence of that high shear stiffness modulus.

Compared to the two other surface characteristics, the effect of the indentation surface characteristic is somehow different. In this case, as shown in **Fig. 20**, it is found that only a small part of the shear span contributes to the resistance of the specimen. The poor bond between concrete and CFRP bars leads to a bending failure of the specimens.

Moreover, those internal strains of concrete show the part of the gross area of concrete that contributes to the performance of those specimens. From **Figs. 18**, **19**, and **20**, the non-uniform internal strain of concrete web is obvious such as a middle axial at section Plane 2 (D/4). The non-uniform pattern of the internal strain of concrete in the web of the beam is the consequence of the circular cross-sectional shape leading to different contributions of CFRP longitudinal reinforcement. Concrete at Plane 1, a middle axial plane of the cross-section of the circular beam contributes more than that at Plane 2 due to the unequal contribution of longitudinal CFRP rebars. In Plane 2, longitudinal reinforcements from the middle axial plane to the extremity of the beam side surface contribute to the resistance of that section when the perfect bond and the ribbed bond model. It is more evident that the internal strain of concrete presents a uniform distribution once Plane 3 is observed. It is the effect of the circular cross-sectional shape of the beam.

6. Conclusions

The main findings of this article can be summarized as follows:

1. Regarding the representative model for the pull-out test, it was observed that smaller indentation and large rib led to a better bond between concrete and FRP bars. Between the two types of nature of FRP reinforcements, reinforcements with ribs present a better bond since it leads to high initial stiffness of 336 N/mm^3 although a poor initial stiffness of 13 N/mm^3 for FRP reinforcement with indentation.
2. The elastic modulus of CFRP reinforcements, on the other hand, does not present a significant effect on the bond-slip curves between FRP bars and concrete, since CFRP bars and GFRP bars present similar bond-slip curves for the same diameter.
3. Bond strength which is the maximum strength in the bond-slip curve reduces with the increase of the diameter of FRP bars. In this study, specimens with a diameter of 12 mm presented the higher bond strength, followed by a diameter of 16 mm and 20 mm.
4. The parametric analysis shows that a poor bond between CFRP bars and concrete leads to bending cracks, which was the case with dented CFRP bars. However, the ribbed CFRP bars led to a better bond between concrete and CFRP, therefore those specimens presented a diagonal shear failure.

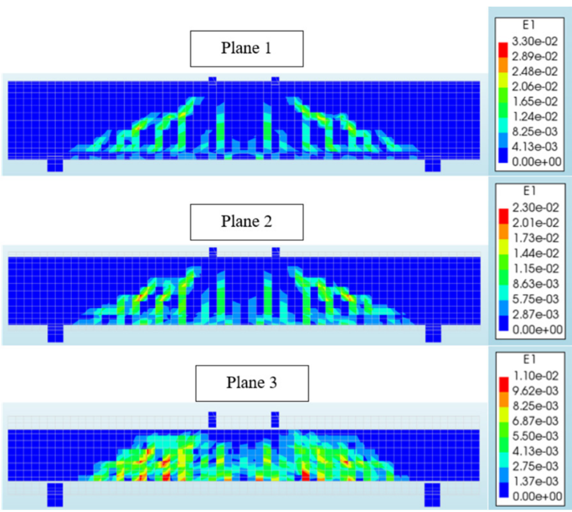

Fig. 19 Internal strain of concrete (BC100 with ribbed bond model).

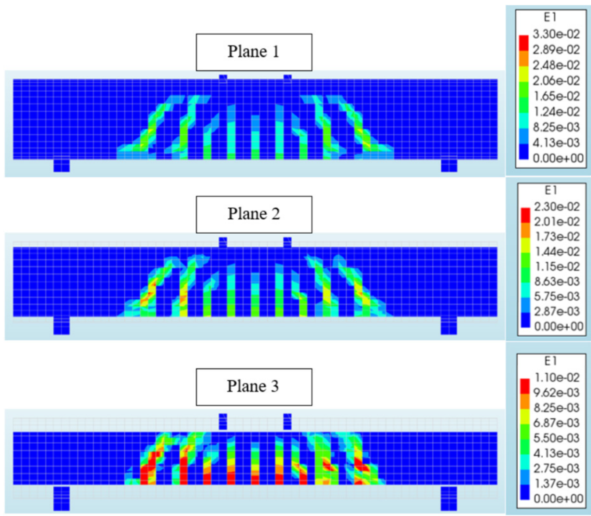

Fig. 20 Internal strain of concrete (BC100 with dented bond model).

5. The internal strain of the circular cross-sectional beam with different bond properties of the longitudinal CFRP rebars showed a non-uniformity as it goes from the surface to the middle axial cross-section of the beam.

Acknowledgements

This research was partially supported by the Japan Society for the Promotion of Science (JSPS), Grant-in-Aid for Scientific Research (B), 19H02226, and Research Committee on Technological Development for Infrastructure in the Ministry of Land, Infrastructure, Transport, and Tourism Kinki Regional Development Bureau.

References

Achillides, Z. and Pilakoutas, K., (2004). "Bond behavior of fiber reinforced polymer bars under direct pullout conditions." *Journal of Composites for Construction*, 8(2), 173-181.

ACI, (2015). "*Guide for the design and construction of structural concrete reinforced with fiber-reinforced polymer (FRP) bars* (ACI440.1R-15)." Farmington Hills, Michigan, USA: American Concrete Institute.

Aiello, M. A., Leone, M. and Pecce, M., (2007). "Bond performances of FRP rebars-reinforced concrete." *Journal of Materials in Civil Engineering*, 19(3), 205-213.

ASTM, (2020). "*Standard test method for bond strength of fiber reinforced polymer matrix composite bars to concrete by pullout testing* (ASTM D7913)." West Conshohocken, Pennsylvania, USA: ASTM International.

Baena, M., Torres, L., Turon, A. and Barris, C., (2009). "Experimental study of bond behaviour between concrete and FRP bars using a pull-out test." *Composites Part B*, 40(8), 784-797.

CNR, (2007). "*Guide for the design and construction of concrete structures reinforced with fiber-reinforced polymer bars* (CNR 203-06)." Rome: National Research Council of Italy (CNR).

CSA, (2012). "*Design and construction of building structures with fibre reinforced polymers* (CSA S806-12)." Toronto: Canadian Standards Association.

El Refai, A., Ammar, M.-A. and Masmoudi R., (2015). "Bond performance of basalt fiber reinforced polymer bars to concrete." *Journal of Composites for Construction*, 19(3), 04014050.

Feenstra, P. H., (1993). "*Computational aspects of biaxial stress in plain and reinforced concrete.*" Thesis (PhD). Delft University of Technology.

fib, (2007). "*FRP reinforcement in RC structures* (*fib* Bulletin 40)." Lausanne, Switzerland: Fédération Internationale du Béton.

Hao, Q., Wang, Y., He, Z. and Ou, J., (2009). "Bond strength of glass fiber reinforced polymer ribbed rebars in normal strength concrete." *Construction and Building Materials*, 23(2), 865-871.

Hordijk, D. A., (1991). "*Local approach to fatigue of concrete.*" Thesis (PhD). Delft University of Technology.

JSCE, (2002). "S*tandard specifications for concrete structures-2002: Structural performance verification*." Tokyo: Japan Society of Civil Engineers.

Mohamed, H. M., Ali, A. H. and Benmokrane, B., (2017). "Behavior of circular concrete members reinforced with carbon-FRP bars and spirals under shear." *Journal of Composites for Construction*, 21(2), 04016090.

Mohamed, H. M. and Benmokrane, B., (2015). "Torsion behavior of concrete beams reinforced with glass fiber-reinforced polymer bars and stirrups." *ACI Structural Journal*, 112(5), 543-552.

Nepomuceno, E., Sena-Cruz, J., Correia, L. and D'Antino, T., (2021). "Review on the bond behavior and durability of FRP bars to concrete." *Construction and Building Materials*, 287, 123042.

Rabotovao, A. M. and Miki, T., (2022). "Influence of surface characteristics of CFRP rebars on behavior of CFRP strengthened RC beams with a circular cross section." *Proceedings of the Japan Concrete Institute*, 44(2), 115-120.

Solyom, S. and Balázs, G. L., (2020). "Bond of FRP bars with different surface characteristics." *Construction and Building Materials*, 264, 119839.

Vecchio, F. J. and Collins, M. P., (1993). "Compression response of cracked reinforced concrete." *ASCE Journal of Structural Engineering*, 119(12), 3590-3610.

Yamaya, A., Nakamura, H. and Nagai, T., (1999). "Shear behavior analyses of RC beams using rotating crack model." *Doboku Gakkai Ronbunshu*, 620/V-43, 187-199. (in Japanese)